Peripheral Choroidal Response to Localized Defocus Blur: Influence of Native Peripheral Aberrations

Dibyendu Pusti, Nimesh B. Patel, Lisa A. Ostrin, Augustine N. Nti, Siddarth Das, and Geunyoung Yoon

College of Optometry, University of Houston, Houston, Texas, United States

Correspondence: Geunyoung Yoon, College of Optometry, University of Houston, Houston, TX 77204, USA; gyoon2@uh.central.edu.

Received: August 21, 2023
Accepted: February 7, 2024
Published: April 5, 2024

Citation: Pusti D, Patel NB, Ostrin LA, Nti AN, Das S, Yoon G. Peripheral choroidal response to localized defocus blur: Influence of native peripheral aberrations. *Invest Ophthalmol Vis Sci.* 2024;65(4):14. https://doi.org/10.1167/iovs.65.4.14

Purpose. This study aims to examine the short-term peripheral choroidal thickness (PChT) response to signed defocus blur, both with and without native peripheral aberrations. This examination will provide insights into the role of peripheral aberration in detecting signs of defocus.

Methods. The peripheral retina (temporal 15°) of the right eye was exposed to a localized video stimulus in 11 young adults. An adaptive optics system induced 2D myopic or hyperopic defocus onto the stimulus, with or without correcting native peripheral ocular aberrations (adaptive optics [AO] or NoAO defocus conditions). Choroidal scans were captured using Heidelberg Spectralis OCT at baseline, exposure (10, 20, and 30 minutes), and recovery phases (4, 8, and 15 minutes). Neural network-based automated MATLAB segmentation program measured PChT changes from OCT scans, and statistical analysis evaluated the effects of different optical conditions over time.

Results. During the exposure phase, NoAO myopic and hyperopic defocus conditions exhibited distinct bidirectional PChT alterations, showing average thickening (10.0 ± 5.3 µm) and thinning (−9.1 ± 5.5 µm), respectively. In contrast, induced AO defocus conditions did not demonstrate a significant change from baseline. PChT recovery to baseline occurred for all conditions. The unexposed fovea did not show any significant ChT change, indicating a localized ChT response to retinal blur.

Conclusions. We discovered that the PChT response serves as a marker for detecting peripheral retinal myopic and hyperopic defocus blur, especially in the presence of peripheral aberrations. These findings highlight the significant role of peripheral oriented blur in cueing peripheral defocus sign detection.

Keywords: myopia, blur detection, peripheral choroidal response, choroidal thickness, peripheral aberration, blur orientation

Myopia is a global concern, affecting more than 30% of the world's population and up to an alarming rate of 92% of the youth population in South and East Asian countries.[1,2] In addition to its significant socioeconomic burden, high myopia increases the risk of ocular pathologies such as retinal disorders, glaucoma, and cataracts.[3–8] Despite numerous efforts by the scientific community to elucidate the underlying mechanisms and develop effective myopia control strategies, a reliable diagnostic biomarker for predicting the onset and progression of myopia has yet to be established.

Recently, studies on both animal models and humans found that the bidirectional subfoveal choroidal layer response to signed defocus signals could be a promising short-term biomarker to study myopia development and control. The findings have indicated that optically induced hyperopic and myopic defocus blur can produce temporary subfoveal choroidal thickness (SFChT) alteration with thinning and thickening, respectively. This phenomenon of defocus-induced choroidal response was first observed in chicken eyes by Wallman et al.,[9] resulting in up to 7 diopters of refraction adjustment by shifting the retina toward the best focal plane. Subsequent studies have also shown SFChT alteration in response to induced retinal defocus.[10–12] For instance, in chick models, Wildsoet and Wallman[10] showed that optical defocus via spectacle lenses caused choroidal and scleral changes, suggesting a mechanism for eye growth regulation. Further investigations in pigmented guinea pigs by Howlett and McFadden[11] demonstrated a similar capacity for spectacle lens compensation, indicating the presence of a conserved mechanism across species. A recent review by Ostrin et al.[12] has explored these dynamics in the context of human myopia, focusing on the choroid's role and potential as a target for therapeutic interventions. Cross-sectional human studies demonstrated similar but considerably smaller magnitude (range 0.37 to 20 µm) of short-term subfoveal choroidal response to induced signed defocus.[12–19] Nonetheless, the underlying mechanisms of the choroidal response to blur and its relationship to long-term myopia development remain unclear.

Along with central vision, peripheral visual feedback plays a crucial role in guiding the regulation of eye growth

Copyright 2024 The Authors

This work is licensed under a Creative Commons Attribution-NonCommercial-NoDerivatives 4.0 International License.

Downloaded from m.iovs.org on 05/02/2024

during emmetropization and myopization.[20,21] Peripheral vision also influences contrast sensitivity[22] and facilitates daily activities like reading, driving, walking, and playing sports.[23,24] However, unlike the defocus-dominated central retina, the peripheral ocular optics are primarily affected by astigmatism and non-rotationally symmetric higher-order aberrations (HOA) like coma. As a result, although blur in the central retina at the fovea leads to rotationally symmetric retinal blur, the intricate interplay of peripheral aberrations produces an oriented or rotationally asymmetric optical blur. Such effects have been previously discussed in relation to optical and neural adaptation[25] and in the context of optical interventions using myopia control contact lenses.[26] It is of growing interest to assess the potential influence of peripheral blur orientation on the detection of defocus and its effect on ocular growth mechanisms. Even though the SFChT response is a well-accepted indicator in myopia development research, little has been known about PChT response to peripheral oriented optical blur.

With this growing interest in understanding the importance of peripheral vision, studying the choroidal response to peripheral optical blur is essential, because it is much more complex than foveal blur. To examine the impact of native peripheral aberrations on the PChT response to different signs of defocus, the present study used an adaptive optics (AO)-based visual simulator to induce defocus independently, with and without peripheral ocular aberrations. Our study aimed to address two fundamental questions: (1) whether the peripheral choroid exhibits a bi-directional response to signed defocus signals, and (2) whether the response varies between induced rotationally symmetric and oriented defocused retinal blur.

Method

Study Participants

Eleven young adults (five male and six female) aged between 26 to 40 years completed the study. Study participants did not have any ocular pathology or undergo ocular surgery and had no history of myopia control interventions. Subjects showing distinctive anterior and posterior barriers in OCT scans were included. They had the best corrected visual acuity of 0.00 logMAR or better, with a mean spherical equivalent of -0.94 ± 1.26D (range 0.46D to -3.53D). All subjects signed the written consent form and willingly participated in the study. The study protocol follows the declaration of Helsinki and was approved by the University of Rochester and the University of Houston's Institutional Review Boards.

Experimental Setup

A custom-built binocular AO system was used to correct or induce desired optical conditions precisely and to deliver the visual stimulus to the peripheral retina. The detailed descriptions of the system can be found elsewhere,[27] while the present system features an upgraded deformable mirror (DM). Briefly, this binocular AO system was constructed with two identical monocular AO channels for each eye. Each monocular AO channel consists of a Shack-Hartmann wavefront sensor (WS), a large-stroke DM (DM97-15, Alpao) and a visual stimulus display or DMD (DLP4710; Texas Instruments, Dallas, TX, USA). A super luminescent diode (SLD; $\lambda = 840$ nm with $\Delta\lambda = 40$ nm) was used as a light source. In the present study, we used only the right arm of the binocular AO setup because this was a monocular experiment. Figure 1 shows a schematic diagram of the experimental setup with the right arm of the AO system. Ocular aberrations are controlled over a 6 mm pupil whereas the visual stimuli were viewed through an artificial pupil set to 5.8 mm. Optical aberrations were corrected and/or defocus was induced continuously in real-time at 12 Hz during the experiment so that optical quality can be reliably maintained. The green optical path in Figure 1 represents the image projection path that merged with a red optical path of the AO setup. To achieve desired visual stimulus delivery, we precisely stimulated the temporal 15° retina while the eye fixates on an external target placed overhead, at the laboratory ceiling. The external fixation was achieved by adding an additional 2″ uncoated pellicle beam splitter in front of the test eye (BS1 in Fig. 1). The fellow eye remained occluded during the study. The peripheral retina was stimulated with a full-color video stimulus, containing a wide range of time-varying spatial frequencies, motion, and contrast, targeting a $\pm 4°$ horizontal and $\pm 3°$ vertical retinal area around the test location with a pixel resolution of 0.276 arcminutes.

Defocus Conditions

We exposed the temporal 15° retina of the right eye to four distinct defocus conditions (Fig. 2). These conditions were designed to induce 2D myopic or hyperopic defocus, with an optional correction for the subject's native peripheral aberrations. The setup ensured the central vision's refractive correction wheras accommodation was controlled with cycloplegia. To instigate the required peripheral optical modifications, we used two separate optical approaches: AO and NoAO defocus conditions. In AO defocus, we undertook real-time corrections for all peripheral lower and higher-order aberrations, allowing a pure defocus induction. On the other hand, the NoAO defocus condition entailed no modifications to peripheral aberrations, instead incorporating the $\pm$2D defocus atop the subject's native peripheral aberrations, following the foveal refractive corrections.

We classified the defocus conditions as follows: (1) NoAO-Myopia: Myopic defocus without peripheral aberration correction, (2) NoAO-Hyperopia: Hyperopic defocus without peripheral aberration correction, (3) AO-Myopia: Myopic defocus with real-time AO correction, and (4) AO-Hyperopia: Hyperopic defocus with real-time AO correction. Figure 2 provides a schematic representation of the induced optical conditions for one of our study subjects, showcasing the reconstructed wavefront maps and convolved letter E for a 6 mm pupil diameter. When observing the NoAO defocus conditions (Figs. 2A, 2B), we noted rotationally asymmetric or oriented retinal images. In contrast, the AO-corrected Pure defocus conditions (Figs. 2C, 2D) produced rotationally symmetric retinal images.

Choroidal Thickness Measurement

The choroidal layer was imaged with enhanced depth imaging OCT technique with Heidelberg Spectralis OCT (Heidelberg Engineering Co, Heidelberg, Germany). Subjects' keratometry reading and refractive errors were incorporated into the system to minimize the image magnification effect due to refraction. Two consecutive scan locations were imaged by using the in-built foveal and temporal fixation targets. Scans were repeated three times using the 30° horizontal line scan with eye tracking (progression

Investigative Ophthalmology & Visual Science

Downloaded from m.iovs.org on 05/02/2024

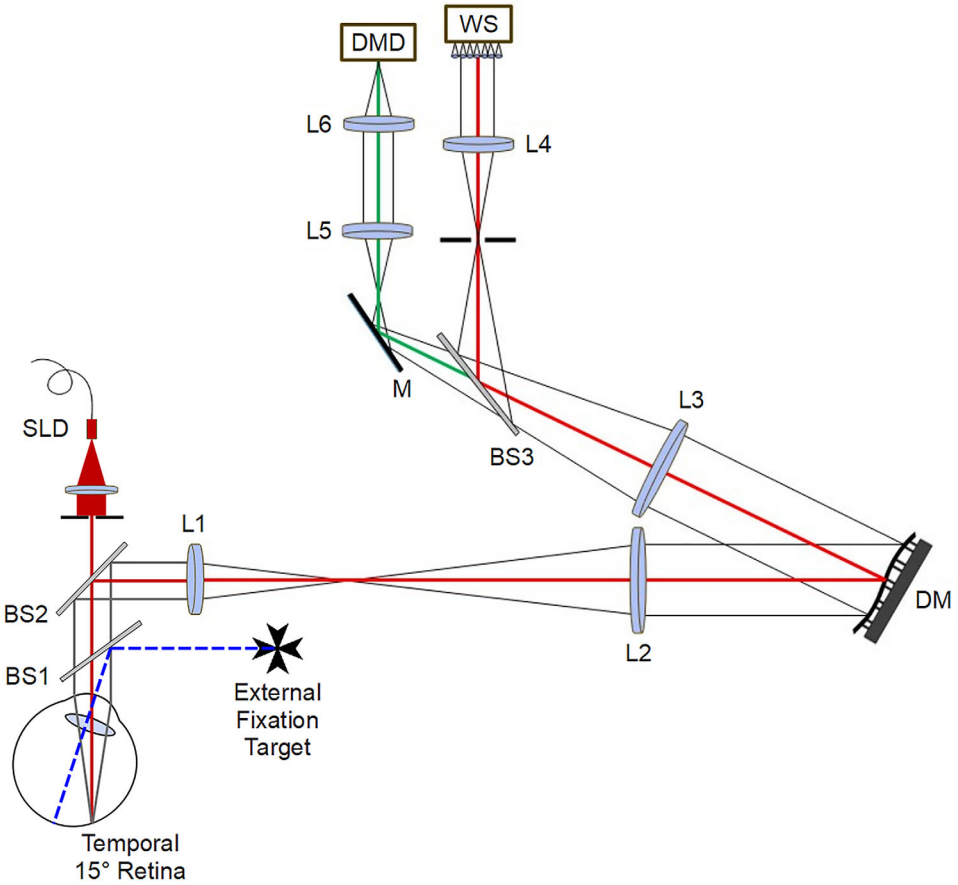

Figure 1. Experimental setup: The right eye fixates to an external fixation target placed at the ceiling, while the fellow eye remains occluded. The custom-built AO device featured a deformable mirror (DM) coupled with a wavefront sensor (WS) for real-time aberration correction. The DLP projector (DMD) displayed the video stimulus to the temporal 15° retina through DM to induce desired optical conditions.

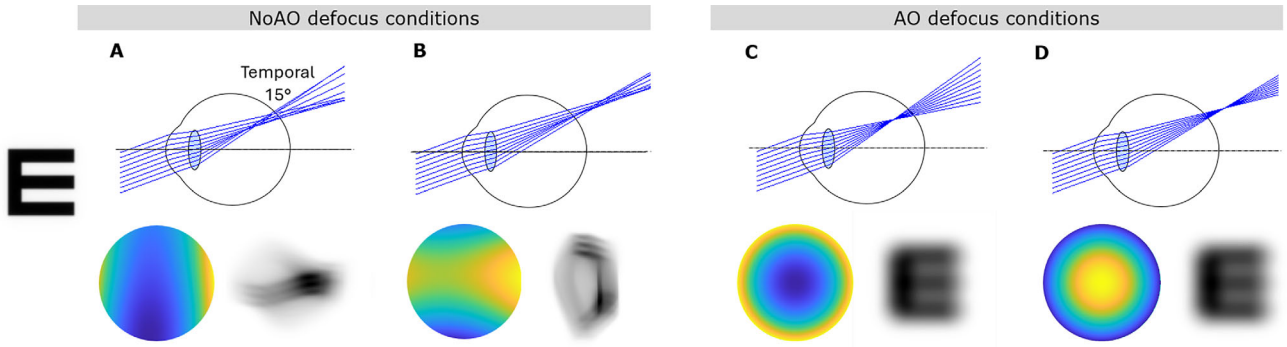

Figure 2. Optical conditions induced in one of our study subjects, using a schematic representation of the eye, along with reconstructed wavefront maps and convolved letter E images for a 6 mm pupil size (plots are not to be scaled). The optical conditions include the following: (**A**) NoAO Myopia: inducing 2D myopic defocus without correcting native aberrations; (**B**) NoAO Hyperopia: inducing 2D hyperopic defocus without correcting native aberrations; (**C**) AO Myopia: 2D pure myopic defocus with AO correction; (**D**) AO Hyperopia: 2D pure hyperopic defocus with AO.

mode) enabled, which ensured scanning at the exact retinal location every time. To obtain high-quality images, 100 frames were averaged with b scan quality maintained above 25 dB. The pixel resolution of each scanned image was 496 × 1536. The images were exported in raw format as .vol files, which preserve all scan parameters, and imported into MATLAB for image processing. The choroidal layer and total retinal thicknesses were automatically segmented using a neural network trained on a DeepLab v3+ network based on ResNet-50.[28,29] The network used was trained on 7676 manually segmented b-scans, from unrelated studies to an accuracy of 99.1% and loss of 0.02. Figure 3 shows a sample image with resultant output and analysis. For each b-scan, boundaries for the inner limiting membrane, retinal pigment

Investigative Ophthalmology & Visual Science

Downloaded from m.iovs.org on 05/02/2024

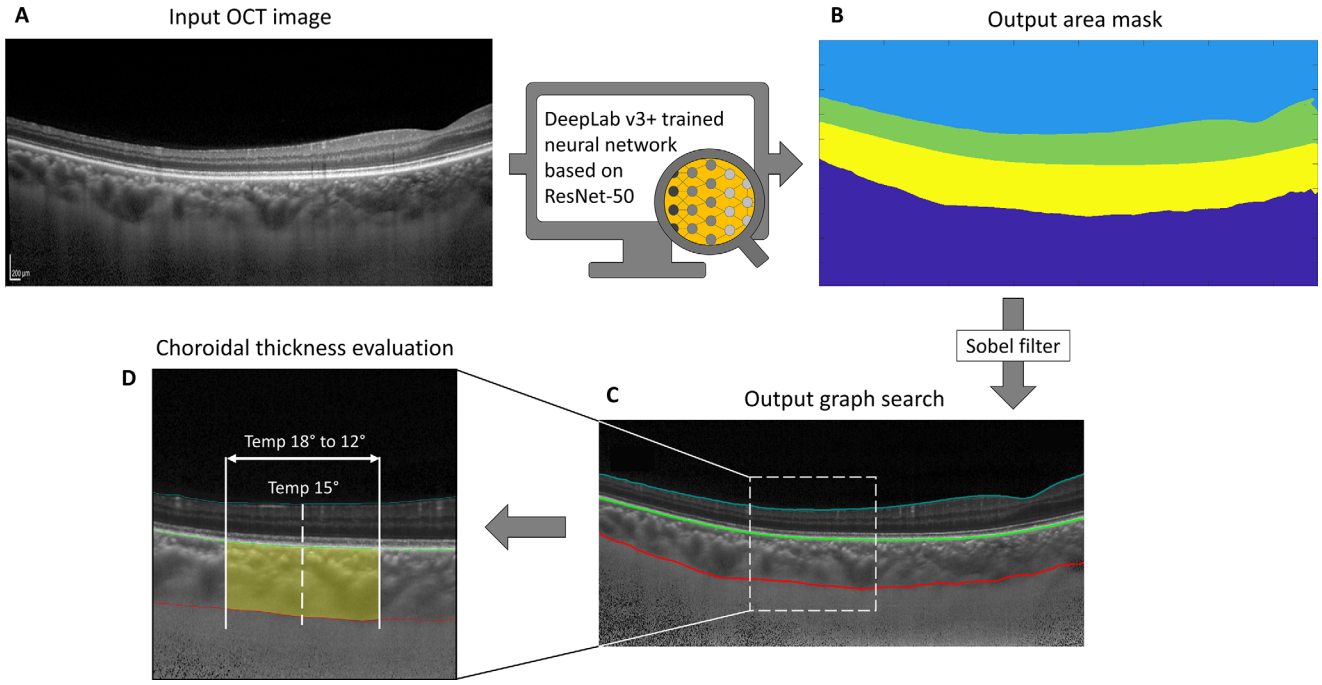

Figure 3. Choroidal thickness assessment from peripheral 30° line scan. Custom-built Matlab program automatically segmented choroidal thickness using a neural network trained on a DeepLab v3+ network based on ResNet-50. The steps are as follows: (**A**) importing raw OCT image; (**B**) outer area mask constructed from the raw OCT image using the trained neural network; (**C**) Sobel filter was applied to construct the final image segmentation using shortest-path graph search; (**D**) mean choroidal thickness was extracted from the exposed retinal region (temporal 18° to 12°).

epithelium, and choroidal–scleral interface were extracted from the semantic segmentation. The boundaries were evaluated for errors and corrected by a trained observer (DP), prior to extracting the PChT. Our neural network segmentation displayed excellent repeatability as demonstrated from repeated scans from a random subject (Supplementary Fig. S2, n = 6, standard deviation = 4.69 µm). Similar delineation approaches were reported before for retinal[30–33] and choroidal[34–36] segmentation from OCT images. We have measured the mean PChT from each pixel location across the exposed horizontal choroidal area with over 240 axial measurements. Though we exposed a horizontal ±4° retinal area around temporal 15°, only ±3° central choroidal area was analyzed (temporal 18° to 12°). This approach maintained a 0.5° margin along both horizontal borders, mitigating potential noise interference. The change from the baseline has been calculated to represent the PChT change at each time point during the exposure and recovery phase. The mean SFChT was evaluated at baseline and during exposure time points using identical OCT scans and segmentation techniques while maintaining central fixation on the OCT device.

Experiment Timeline and Procedure

After the subject's right eye was administered 1% tropicamide and 2.5% phenylephrine for pupil dilation, they waited for 30 minutes to attain cycloplegia. After this, baseline peripheral choroidal scans were obtained. The subjects were then positioned in front of the AO system, and a careful alignment process was undertaken to align the subject's right eye pupil with the system's optical axis. The left eye was occluded during the entire session. Foveal refractive errors were then corrected using the phoropter integrated within the AO system. Next, they were asked to fixate at an external laser point reflection with the right eye through a high transmittance large 2-inch pellicle beam splitter. At this point, the exposure phase was initiated with the implementation of one of the four randomly selected optical conditions. The subjects' foveal fixation was continuously monitored with a dedicated pupil camera while the AO systems ran in real-time to project the video stimulus at the temporal 15° retinal eccentricity. Supplementary Figure S1 shows the reliability of the real-time AO correction in one of the study participants. OCT scans were repeated at 10, 20, and 30 minutes within the exposure phase. To minimize the exposure interval and ensure a swift transition between the instruments, the OCT machine was strategically positioned adjacent to the AO setup. The subjects were instructed to keep their eyes closed while being navigated by the researcher (D.P.) to the OCT machine from the AO system. Maintaining a dark room condition, the OCT scans were efficiently completed within a span of three to four minutes. The 15 minutes of recovery phase was initiated immediately after the exposure phase, where OCT scans were achieved at 4, 8, and 15 minutes. At least 24 hours were allowed between two sessions, and measurements were scheduled at the same time frame for each session to avoid unwanted ChT fluctuation due to diurnal variation.

Statistical Analysis

To investigate the effects of different optical conditions on choroidal thickness over time, a two-factor repeated measures analysis of variance (ANOVA) was conducted. The factors examined were "Optical Conditions" (with four

Investigative Ophthalmology & Visual Science

Downloaded from m.iovs.org on 05/02/2024

levels: NoAO-Myopia, NoAO-Hyperopia, AO-Myopia, and AO-Hyperopia) and "Time" (with seven levels: 0, 10, 20, 30, 34, 38, and 45 minutes). After conducting the repeated measures ANOVA, we performed pairwise comparisons using Tukey's post hoc analysis. This analysis allowed us to examine the specific differences in ChT at different time points compared to the baseline for each optical condition (where time was treated as a fixed factor). Additionally, we assessed the differences between optical conditions for each time point during the exposure phase (treating optical conditions as a fixed factor). All statistical analyses were conducted using SPSS version 26 (IBM Corp., Armonk, NY, USA). The statistical significance level was set at $P < 0.05$ to determine the presence of significant differences.

Results

Ocular Aberrations

Aberration data from eleven subjects were collected using the Shack-Hartmann sensor of the AO device for the 6 mm pupil diameter at both foveal and peripheral test locations. To present the aberration data in clinical terminology, the lower-order Zernike terms were converted to dioptric components. The Zernike defocus (Z_2^0) value was converted to dioptric power corresponding to spherical equivalent (M) and J0 and J45 astigmatic components were converted from vertical (Z_2^2) and oblique (Z_2^{-2}) astigmatic components, respectively. At the fovea, the mean defocus was found to be −0.94 ± 1.26D (range 0.46D to −3.53D), and the average peripheral defocus (at temp 15°) was −0.81D ± 1.29D (range 0.21D to −3.94D). Our subjects showed a wide range of astigmatism at the fovea as J0 = −0.48D ± 0.63D, J45 = −0.08D ± 0.20D. Upon foveal correction, the peripheral relative J0 astigmatic component was ranging from 1.60D to −0.73D and J45 from 0.29D to −0.16D. Table 1 provides a summary of each subject's foveal and relative peripheral lower-order aberrations (LOA in diopters) after foveal refractive correction.

At the fovea, the root mean square (RMS) HOAs showed a mean value of 0.51 ± 0.11 µm (range: 0.71 to 0.34 µm). In contrast, when examining the periphery, we observed that peripheral HOARMS exhibited a higher mean value of 0.57 ± 0.34 µm (range: 1.46 to 0.07 µm). The dominant aberrations of HOARMS were horizontal coma (Z_3^1) and primary spherical aberration (Z_4^0). The specific values for peripheral aberrations were as follows: mean Z_3^1 of 0.07 ± 0.26 µm (range 0.36 to −0.41 µm) and mean Z_4^0 of 0.11 ± 0.22 µm (range 0.38 to −0.39 µm). These findings highlight a notable increase in HOAs in the peripheral vision compared to the foveal region. Table 2 provides a summary of each subject's foveal and peripheral HOAs, whereas Supplementary Table S1 provides detailed peripheral LOA and HOA up to fourth-order Zernike polynomial.

Table 1. Lower Order Aberrations: Summary of Each Subject's Foveal and Peripheral (Temporal 15°) Dioptric Components

	Foveal LOA (D)			Relative Peripheral LOA (D)		
Subject ID	M	J0	J45	M	J0	J45
Sub01	0.07	0.07	−0.03	0.08	0.22	0.29
Sub02	−1.17	−0.28	0.06	−0.32	−0.14	−0.13
Sub03	0.07	−0.34	−0.09	−0.03	−0.21	0.04
Sub04	−2.18	0.39	−0.59	1.57	−0.63	0.16
Sub05	−0.69	−0.15	0.00	0.10	−0.14	0.03
Sub06	−0.65	−1.01	−0.07	−1.60	−0.73	0.00
Sub07	−2.40	−1.65	−0.13	2.32	1.60	0.16
Sub08	−0.01	−0.03	0.03	−0.52	−0.39	−0.13
Sub09	0.46	−1.31	−0.22	−0.33	1.34	0.10
Sub10	−3.53	−0.82	−0.01	−0.41	−0.04	−0.11
Sub11	−0.32	−0.16	0.20	0.53	−0.06	−0.16

Peripheral Choroidal Response

The study aimed to evaluate the peripheral choroidal response by measuring the change in PChT from the baseline measurement (Fig. 4A). In the case of NoAO myopic conditions, there was a significant increase in peripheral choroidal thickening at 20 minutes (12.5 ± 4.9 µm, $P < 0.001$) and 30 minutes (10.3 ± 7.4 µm, $P < 0.01$). This led to an overall average rise of 10.0 ± 5.3 µm during the exposure phase, considering the mean peripheral choroidal thickness over the 10-, 20-, and 30-minute intervals. On the other hand, the NoAO hyperopic defocus exhibited an opposite trend, showing an average choroidal thinning of −9.1 ± 5.5 µm across the exposure phase. However, only the 20-minute exposure phase displayed a statistically significant difference from the baseline choroidal thickness (−11.7 ± 3.9 µm, $P = 0.05$). Overall, the NoAO defocus conditions demonstrated a clear bidirectional trend in PChT alteration over the exposure phase. In contrast, both AO myopic and hyperopic defocus conditions showed much

Table 2. HOAs: Summary of Each Subject's Foveal and Peripheral (Temporal 15°) HOAs for 6 mm Pupil

	Foveal HOA [µm]			Peripheral HOA [µm]		
Subject ID	Horizontal Coma (Z_3^1)	Spherical Aberration (Z_4^0)	HOA RMS	Horizontal Coma (Z_3^1)	Spherical Aberration (Z_4^0)	HOA RMS
Sub01	0.11	0.45	0.60	0.26	0.31	0.53
Sub02	−0.21	0.01	0.38	−0.41	0.06	0.62
Sub03	−0.09	0.30	0.45	0.01	0.38	0.60
Sub04	0.18	0.31	0.47	0.49	0.32	0.69
Sub05	−0.01	0.22	0.34	0.20	0.13	0.37
Sub06	−0.11	0.21	0.53	−0.08	−0.39	1.46
Sub07	−0.02	−0.03	0.48	−0.01	0.04	0.07
Sub08	0.39	0.10	0.67	0.13	0.10	0.68
Sub09	0.28	0.02	0.56	0.06	−0.08	0.35
Sub10	−0.33	−0.06	0.71	−0.21	0.05	0.39
Sub11	0.33	0.18	0.44	0.36	0.24	0.49

Investigative Ophthalmology & Visual Science

Downloaded from m.iovs.org on 05/02/2024

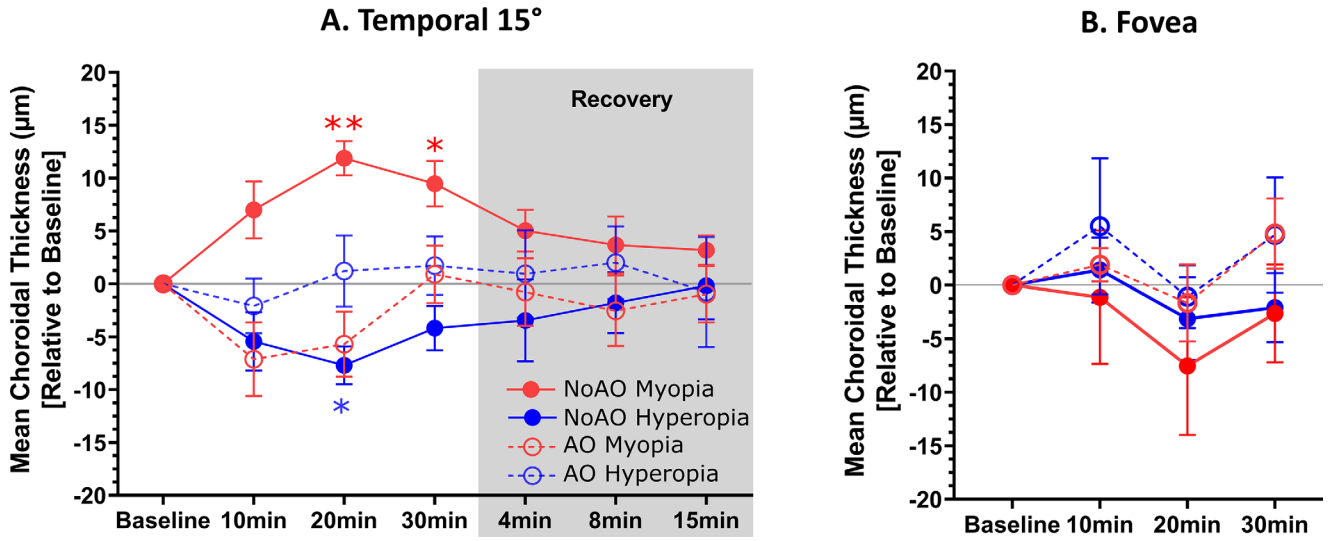

Figure 4. Relative mean changes in choroidal thickness from the baseline value in the (**A**) peripheral test location (temporal 15°) and (**B**) at the fovea. The gray-shaded area indicates the peripheral choroidal recovery phase that occurred during the 15-minute period immediately after the exposure phase. The *error bars* represent the standard error of the mean, whereas statistically significant deviations are denoted by *asterisks* (*$P < 0.05$, **$P < 0.005$). For detailed statistical analysis data, please refer to Supplementary Table S2.

lower PChT alteration with no statistically significant difference from the baseline. The AO myopic condition exhibited a trend of choroidal thinning at both 10 and 20 minutes during the exposure phase, while the AO hyperopic condition did not show a significant deviation from the baseline PChT at any time point. For additional information and statistical analysis, please refer to Supplementary Table S2, which presents post hoc multivariate regression analysis between all measurement time points for each optical test condition.

During the exposure phase, we analyzed the data using repeated measure ANOVA, revealing two key findings. First, there was a significant overall effect of the induced optical conditions on mean PChT measurements ($F_{2.2,22.3} = 17.592$, $P = 0.000$), indicating varying changes in peripheral choroidal thickness depending on the specific defocus condition. Second, we observed a significant overall interaction between time and induced optical conditions on mean PChT measurements ($F_{4.3,43.2} = 7.075$, $P = 0.000$), suggesting that the impact of induced defocus on PChT varied over time during the exposure phases.

We performed further analysis to investigate the interaction of PChT among each induced optical condition at individual time points during the exposure phase. The mean PChT data for the 10-, 20-, and 30-minute exposure periods are plotted in Figure 5, revealing statistically significant differences among the induced optical conditions at these specific exposure time points. Specifically, the NoAO myopic and NoAO hyperopic conditions displayed significant differences at all exposure time points ($P = 0.029$, 0.000, and 0.000 for 10, 20, and 30 minutes, respectively), and similarly, the NoAO and AO myopic defocus conditions showed significant differences at all time points ($P = 0.013$, 0.000, and 0.045 for 10, 20, and 30 minutes, respectively). However, no significant differences were observed between AO defocus conditions at any time points. For more detailed information on the multivariate regression analysis between optical test conditions and each measurement time point for the peripheral test location, please refer to Supplementary Table S3.

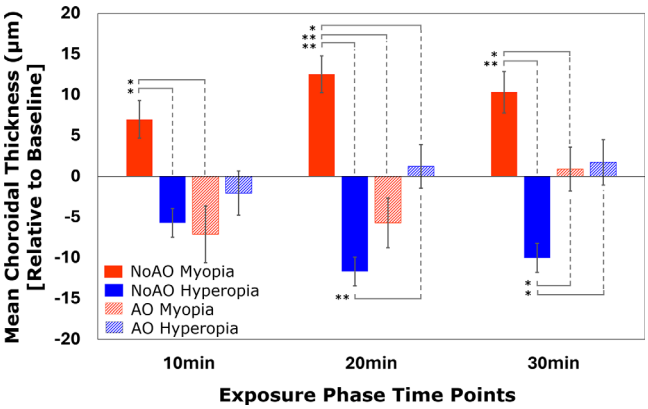

Figure 5. The alterations in peripheral choroidal thickness relative to the baseline (same data as in Figure 4), focused on significant differences among the optical test conditions at 10, 20, and 30 minutes of exposure. The *error bars* represent the standard error of the mean, with *asterisks* denoting statistically significant deviations (*$P < 0.05$, **$P < 0.005$). For a more detailed statistical analysis, please refer to Supplementary Table S3.

The recovery of PChT was measured at 4, 8, and 15 minutes immediately after the exposure phase for all test conditions. Gradual recovery to the baseline data was observed for all test conditions, and none of the recovery points showed a statistically significant difference from the baseline. The average PChT recovery at 15 minutes was 3.18 ± 8.20 µm, −0.19 ± 8.46 µm, −0.97 ± 11.97 µm, and −0.77 ± 11.68 µm for NoAO myopia, NoAO hyperopia, AO myopia, and AO hyperopia, respectively. Table 3 summarizes the absolute PChT values throughout the study period for all test conditions, and Figure 4 shows the PChT alteration relative to the baseline values during the exposure and recovery phase for all test conditions.

In Figure 4B, the unexposed mean SFChT is shown relative to the baseline values, and did not exhibit any statistically significant alterations. However, during the exposure

Investigative Ophthalmology & Visual Science

Downloaded from m.iovs.org on 05/02/2024

Table 3. Absolute Peripheral Choroidal Thickness: Measured Throughout the Study Period for All Test Conditions

	NoAO-Myopia (Mean ± SD)	NoAO-Hyperopia (Mean ± SD)	AO-Myopia (Mean ± SD)	AO-Hyperopia (Mean ± SD)
Baseline	264.86 ± 65.88	277.37 ± 63.14	274.77 ± 64.40	276.86 ± 73.67
Exposure phase				
10 min	271.85 ± 65.53	271.65 ± 62.62	267.65 ± 61.86	274.78 ± 76.81
20 min	277.38 ± 66.52	265.67 ± 63.03	269.06 ± 66.63	278.07 ± 72.16
30 min	275.18 ± 63.94	267.37 ± 62.67	275.66 ± 65.29	278.58 ± 76.58
Recovery phase				
4 min	269.88 ± 65.68	272.18 ± 60.26	273.99 ± 65.36	277.80 ± 82.12
8 min	268.52 ± 69.12	273.86 ± 59.54	272.22 ± 65.79	278.86 ± 79.39
15 min	268.03 ± 65.63	275.45 ± 55.90	273.79 ± 60.77	276.08 ± 87.19

The standard deviation represents intra-subject variability at each time point. All values are in µm.

Table 4. Absolute Subfoveal Choroidal Thickness: Measured Throughout the Exposure Phase for All Test Conditions

	NoAO-Myopia (Mean ± SD)	NoAO-Hyperopia (Mean ± SD)	AO-Myopia (Mean ± SD)	AO-Hyperopia (Mean ± SD)
Baseline	320.46 ± 41.84	318.50 ± 49.96	319.95 ± 40.02	310.87 ± 43.69
Exposure phase				
10 min	319.33 ± 42.63	319.91 ± 48.01	321.85 ± 39.77	316.37 ± 41.96
20 min	312.91 ± 36.50	315.38 ± 48.91	318.30 ± 44.62	309.78 ± 39.91
30 min	317.82 ± 36.47	316.41 ± 44.69	324.76 ± 35.48	315.55 ± 44.01

The standard deviation represents intrasubject variability at each time point. All values are in µm.

phase, the mean SFChT changed by −3.77 ± 17.22 µm, −1.27 ± 8.84 µm, 1.68 ± 6.20 µm, and 3.03 ± 14.00 µm for NoAO myopia, NoAO hyperopia, AO myopia, and AO hyperopia, respectively. Table 4 summarizes all the absolute sub-foveal ChT values for each test condition throughout the exposure phase.

Discussion

Our study aimed to investigate the impact of locally induced AO and NoAO defocus blur on peripheral choroidal thickness in healthy young individuals. We found a bidirectional response in PChT to short-term hyperopic and myopic blur induction. Specifically, inducing hyperopic blur resulted in a decrease in peripheral choroidal thickness, while inducing myopic blur led to an increase (Fig. 4A). Interestingly, the bidirectional response manifested distinctly when individuals retained their native peripheral aberrations (such as astigmatism and coma) during defocus induction. However, contrasting this, under AO defocus conditions (accompanied by real-time aberration correction), the choroid exhibited a tendency toward thinning with induced AO myopia, accompanied by minimal change during hyperopic defocus. As such, the AO defocus conditions showcased a lack of substantial thickness alteration or bidirectional response. This insight suggests that the peripheral visual system is more adept at discerning between myopic and hyperopic defocus signals in the presence of blur orientation cues.

Now the question arises: why is the peripheral visual system sensitive to oriented blur? The potential answer lies in two factors.

Factor 1: Role of Peripheral Ocular Optics

Because of the presence of peripheral astigmatism and radially asymmetric higher-order aberrations, such as coma, the peripheral retina always experiences a specific blur orientation pattern during emmetropization, which systematically changes with accommodation and disaccommodation. Therefore the peripheral visual system learns to detect the sign of defocus in the presence of one's own peripheral blur orientations. Previous studies have well established that the brain adapts to individual retinal blur and learns to process images accordingly.[37–39] To thoroughly assess the role of peripheral blur orientation cues, we used our AO visual simulator to test the peripheral retina's response to defocus signs, both with and without this cue. Our study used natural scene video stimuli adhering to the 1/f spectral characteristic, focusing predominantly on low spatial frequencies.[40–42] Our findings revealed a pronounced decline in choroidal response when innate peripheral blur orientation cues were absent, emphasizing their critical role in defocus detection. Additionally, our experiments showed that the AO correction (both LOA and HOA), targeting both lower- and higher-order aberrations, significantly affected the lower spatial frequency range of the defocused video stimulus, particularly below 10 cycles/degree. This aligns with the findings of Swiatczak and Schaeffel,[13] where subfoveal choroidal thickness was shown to be influenced by movies featuring spatial frequencies exclusively under 10 cyc/deg.

Factor 2: The Structural Configuration of the Peripheral Retinal Layers

The peripheral retina is populated by ganglion cells with radially elongated receptive fields that are orientation sensitive. As a result, ganglion cells in the peripheral retina tend to be more sensitive to stimuli that are aligned with parallel or perpendicular to the retinal meridians and less sensitive to stimuli that are oblique or diagonal to these meridians.[43–46]

Investigative Ophthalmology & Visual Science

Downloaded from m.iovs.org on 05/02/2024

Previous studies have reported bidirectional compensatory alterations in choroidal thickness in response to defocused blur, mainly in the subfoveal choroidal layer. Human studies have demonstrated choroidal thickness changes ranging from 0.37 to 20 µm when the fovea is exposed to 2D to 3D myopic and hyperopic defocus for up to two hours.[16–18] However, to the best of our knowledge no previous literature reported the response of the peripheral choroidal layer to localized blur signals. In our study, we induced 2D myopic and hyperopic defocus and observed a two-way PChT alteration with changes of up to 29.14 µm during the exposure phase, adding new insights to the existing literature.

The diverse optics and structural integrity of the fovea and peripheral retina can lead to differential responses to oriented or astigmatic defocus blur. A study by Yazdi et al.[18] examined induced short-term astigmatic myopic defocus at the subfoveal choroidal layer and found that myopic defocus blur induces a higher choroidal response (thickening) compared to induced astigmatic blur. In contrast, our study's peripheral choroidal response exhibited an opposite trend to the subfoveal choroid, suggesting greater sensitivity to blur orientation cues in the periphery. Thus this might suggest that the mechanism for detecting defocus blur sign in the peripheral retina when exposed to oriented blur may differ from that in the foveal region. Prior research has also explored the orientation of peripheral image blur's potential significance in peripheral defocus detection.[47]

The unexposed sub-foveal choroid in our subjects did not deviate significantly from baseline during the exposure phase (Fig. 4B), indicating a regional choroidal response to the induced visual signals. Hoseini-Yazdi et al.[48] conducted a study that reported an alteration in regional choroidal thickness, which supports this finding. We still do not fully understand how visual blur causes changes in choroidal thickness, which makes it difficult to determine the role of neural adaptation to native peripheral aberrations in guiding these changes. It is more sensible to speculate that the peripheral retina's dominance of radially elongated receptive fields may make it locally more sensitive to oriented blur than to radially symmetric blur.

The rapid alteration of choroidal layer thickness after exposure to defocus blur poses an intriguing question. Comprising primarily of blood vessels, the human choroidal layer accounts for approximately 80% to 85% of its total volume, making variations in choroidal thickness a potential marker for changes in choroidal blood flow.[14,49] Speculations on the potential mechanism of choroidal response to defocus blur signals have been based on molecular biology genomics and choroidal perfusion studies.[50–52] To better understand the relationship between retinal blur and choroidal blood flow, it's essential to consider the local molecular reactions in response to blurred images. This process starts with the reception of blurred images by the retina, decoding the sign of defocus and extends to the rapid change in choroidal blood circulation, significantly influencing choroidal thickness. However, the specific impact of different retinal blur conditions on metabolic demands and choroidal blood supply, and consequently choroidal thickness alteration, remains unclear.

Followed by the exposure phase, we also looked at the PChT recovery, and we observed a rapid and substantial 94% to 98% recovery of PChT within 15 minutes, across various induced optical conditions in our study participants. The lack of existing peripheral choroidal thickness recovery data in the literature adds significance to our findings. To contextualize this phenomenon, we plan to compare it with available subfoveal choroidal thickness recovery data. Notably, Delshad et al.[53] reported a similar trend of SFChT recovery, with complete recovery observed within 21 and 35 minutes after removing hyperopic and myopic defocus, respectively. However, studies also found variable results when investigating complete recovery over up to two hours.[16]

Our study was limited by sample size because of the need for a relatively long time commitment for each subject to make over multiple measurement sessions. Although we noticed bidirectional PChT alteration with NoAO defocus conditions, increasing the sample size is not just increasing a significance level of the finding but also, nonsignificant findings in both NoAO and AO defocus conditions could become significant. Additionally, the limited sample size may have affected our ability to discern the differences in defocus-induced choroidal thickness responses between myopic and non-myopic subjects. Prior research has shown divergent subfoveal choroidal responses in emmetropic and myopic individuals, suggesting a potential area of discrepancy that our study might not have adequately captured.[13] We excluded participants with ocular or systemic illness and conducted measurements at the same time of day to control for diurnal variation. However, there could still be differences in ocular and choroidal metabolic activities between subjects that could cause intersubject variability.

Conclusions

In conclusion, our study found that the choroidal layer in the periphery exhibited thickness changes in response to both myopic and hyperopic defocus. Specifically, when retinal blur was oriented, induced myopic defocus caused choroidal thickening, whereas hyperopic defocus caused thinning. We hypothesize that the orientated peripheral retinal blur caused by peripheral asymmetric aberrations plays an important role in signaling choroidal thickness changes in response to signed defocus blur. Future research is needed to further test this hypothesis, to investigate the choroidal signaling pathways that are selectively triggered by different orientations of blur signals at different peripheral retinal locations, and to improve our understanding of the potential contribution of the peripheral blur to central eye growth.

Acknowledgments

We thank Meta for the generous support of an unrestricted grant. We are thankful to all our study participants.

Supported by the National Institutes of Health (R01EY034151).

Disclosure: **D. Pusti,** None; **N.B. Patel,** None; **L.A. Ostrin,** None; **A.N. Nti,** None; **S. Das,** None; **G. Yoon,** None

References

1. Rudnicka AR, Kapetanakis VV, Wathern AK, et al. Global variations and time trends in the prevalence of childhood myopia, a systematic review and quantitative meta-analysis: Implications for aetiology and early prevention. *Br J Ophthalmol.* 2016;100:882–890.

Investigative Ophthalmology & Visual Science

Downloaded from m.iovs.org on 05/02/2024

2. Holden BA, Fricke TR, Wilson DA, et al. Global prevalence of myopia and high myopia and temporal trends from 2000 through 2050. *Ophthalmology*. 2016;123:1036–1042.
3. Mehdizadeh M, Ashraf H. Prevalence of cataract type in relation to axial length in subjects with high myopia and emmetropia in an Indian population. *Am J Ophthalmol*. 2008;146:329–330.
4. Dragoumis I, Richards A, Alexander P, Poulson A, Snead M. Retinal detachment in severe myopia. *The Lancet*. 2017;390:124.
5. Polkinghorne PJ, Craig JP. Northern New Zealand rhegmatogenous retinal detachment study: epidemiology and risk factors. *Clin Exp Ophthalmol*. 2004;32:159–163.
6. Li X, Beijing Rhegmatogenous Retinal Detachment Study Group. Incidence and epidemiological characteristics of rhegmatogenous retinal detachment in Beijing, China. *Ophthalmology*. 2003;110:2413–2417.
7. Vongphanit J, Mitchell P, Wang JJ. Prevalence and progression of myopic retinopathy in an older population. *Ophthalmology*. 2002;109:704–711.
8. Mitchell P, Hourihan F, Sandbach J, Jin Wang J. The relationship between glaucoma and myopia. *Ophthalmology*. 1999;106:2010–2015.
9. Wallman J, Wildsoet C, Xu A, et al. Moving the retina: choroidal modulation of refractive state. *Vision Res*. 1995;35:37–50.
10. Wildsoet C, Wallman J. Choroidal and scleral mechanisms of compensation for spectacle lenses in chicks. *Vision Res*. 1995;35:1175–1194.
11. Howlett MHC, McFadden SA. Spectacle lens compensation in the pigmented guinea pig. *Vision Res*. 2009;49:219–227.
12. Ostrin LA, Harb E, Nickla DL, et al. IMI—the dynamic choroid: new insights, challenges, and potential significance for human myopia. *Invest Ophthalmol Vis Sci*. 2023;64:4–4.
13. Swiatczak B, Schaeffel F. Emmetropic, but not myopic human eyes distinguish positive defocus from calculated blur. *Invest Ophthalmol Vis Sci*. 2021;62:14–14.
14. Swiatczak B, Schaeffel F, Calzetti G. Imposed positive defocus changes choroidal blood flow in young human subjects. *Graefes Arch Clin Exp Ophthalmol*. 2023;61:115–125.
15. Chiang STH, Phillips JR, Backhouse S. Effect of retinal image defocus on the thickness of the human choroid. *Ophthalmic Physiol Opt*. 2015;35:405–413.
16. Wang D, Chun RK, Liu M, et al. Optical defocus rapidly changes choroidal thickness in schoolchildren. *PLoS One*. 2016;11:1–12.
17. Chiang STH, Chen TL, Phillips JR. Effect of optical defocus on choroidal thickness in healthy adults with presbyopia. *Invest Ophthalmol Vis Sci*. 2018;59:5188–5193.
18. Hoseini-Yazdi H, Vincent SJ, Read SA, Collins MJ. Astigmatic defocus leads to short-term changes in human choroidal thickness. *Invest Ophthalmol Vis Sci*. 2020;61:4–11.
19. Delshad S, Collins MJ, Read SA, Vincent SJ. The human axial length and choroidal thickness responses to continuous and alternating episodes of myopic and hyperopic blur. *PLoS One*. 2020;15(12):e0243076.
20. Smith EL, Kee CS, Ramamirtham R, Qiao-Grider Y, Hung LF. Peripheral vision can influence eye growth and refractive development in infant monkeys. *Invest Ophthalmol Vis Sci*. 2005;46:3965–3972.
21. Smith EL. Prentice award lecture 2010: a case for peripheral optical treatment strategies for myopia. *Optom Vis Sci*. 2011;88:1029–1044.
22. Venkataraman AP, Papadogiannis P, Romashchenko D, Winter S, Unsbo P, Lundström L. Peripheral resolution and contrast sensitivity: effects of monochromatic and chromatic aberrations. *J Opt Soc Am A Opt Image Sci Vis*. 2019;36:B52.
23. Ortiz-Peregrina S, Casares-López M, Castro-Torres JJ, Anera RG, Artal P. Effect of peripheral refractive errors on driving performance. *Biomed Opt Express*. 2022;13:5533.
24. Vater C, Wolfe B, Rosenholtz R. Peripheral vision in real-world tasks: a systematic review. *Psychon Bull Rev*. 2022;29:1531–1557.
25. Zheleznyak L, Barbot A, Ghosh A, Yoon G. Optical and neural anisotropy in peripheral vision. *J Vis*. 2016;16:1–11.
26. Ji Q, Yoo YS, Alam H, Yoon G. Through-focus optical characteristics of monofocal and bifocal soft contact lenses across the peripheral visual field. *Ophthalmic Physiol Opt*. 2018;38:326–336.
27. Sabesan R, Zheleznyak L, Yoon G. Binocular visual performance and summation after correcting higher order aberrations. *Biomed Opt Express*. 2012;3:3176.
28. Chen L-C, Papandreou G, Schroff F, Adam H. Rethinking atrous convolution for semantic image segmentation. *arXiv preprint arXiv* 170605587, 2017.
29. He K, Zhang X, Ren S, Sun J. Deep residual learning for image recognition. *Proc IEEE Comp Soc Conference on Computer Vision and Pattern Recognition*. 2016:770–778.
30. Srinivasan VV, Das S, Patel N. Widefield OCT imaging for quantifying inner retinal thickness in the nonhuman primate. *Transl Vis Sci Technol*. 2022;11:1–12.
31. Roy AG, Conjeti S, Karri SP, et al. ReLayNet: retinal layer and fluid segmentation of macular optical coherence tomography using fully convolutional networks. *Biomed Opt Express*. 2017;8:3627.
32. Venhuizen FG, van Ginneken B, Liefers B, et al. Robust total retina thickness segmentation in optical coherence tomography images using convolutional neural networks. *Biomed Opt Express*. 2017;8:3292.
33. Kugelman J, Alonso-Caneiro D, Read SA, Vincent SJ, Collins MJ. Automatic segmentation of OCT retinal boundaries using recurrent neural networks and graph search. *Biomed Opt Express*. 2018;9:5759.
34. Kugelman J, Alonso-Caneiro D, Read SA, et al. Automatic choroidal segmentation in OCT images using supervised deep learning methods. *Sci Rep*. 2019;9:1–13.
35. Chen HJ, Huang YL, Tse SL, et al. Application of artificial intelligence and deep learning for choroid segmentation in myopia. *Transl Vis Sci Technol*. 2022;11:1–10.
36. Hsia WP, Tse SL, Chang CJ, Huang YL. Automatic segmentation of choroid layer using deep learning on spectral domain optical coherence tomography. *Appl Sci*. 2021;11:5488.
37. Sawides L, de Gracia P, Dorronsoro C, Webster MA, Marcos S. Vision is adapted to the natural level of blur present in the retinal image. *PLoS One*. 2011;6:1–6.
38. Artal P, Chen L, Fernández EJ, Singer B, Manzanera S, Williams DR. Neural compensation for the eye's optical aberrations. *J Vis*. 2004;4:4–4.
39. Mon-Williams M, Tresilian JR, Strang NC, Kochhar P, Wann JP. Improving vision: neural compensation for optical defocus. *Proc R Soc B Biol Sci*. 1998;265:71–77.
40. van Hateren JH. Theoretical predictions of spatiotemporal receptive fields of fly LMCs, and experimental validation. *J Comp Physiol*. 1992;171:157–170.
41. Field DJ. Relations between the statistics of natural images and the response properties of cortical cells. *J Opt Soc Am A*. 1987;4:2379.
42. Tolhurst DJ, Tadmor Y, Chao T. Amplitude spectra of natural images. *Ophthalmic Physiol Opt*. 1992;12:229–232.
43. Mathur A, Gehrmann J, Atchison DA. Pupil shape as viewed along the horizontal visual field. *J Vis*. 2013;13:1–8.

Investigative Ophthalmology & Visual Science

Downloaded from m.iovs.org on 05/02/2024

44. Levick WR, Thibos LN. Analysis of orientation bias in cat retina. *J Physiol*. 1982;329:243–261.
45. Cuenca N, Lopez S, Howes K, Kolb H. Two types of orientation-sensitive responses of amacrine cells in the mammalian retina. *Nature*. 1991;350(6316):347–350.
46. Passaglia CL, Troy JB, Rüttiger L, Lee BB. Orientation sensitivity of ganglion cells in primate retina. *Vision Res*. 2002;42:683–694.
47. Zheleznyak L. Peripheral optical anisotropy in refractive error groups. *Ophthalmic Physiol Opt*. 2023;43: 435–444.
48. Hoseini-Yazdi H, Vincent SJ, Collins MJ, Read SA. Regional alterations in human choroidal thickness in response to short-term monocular hemifield myopic defocus. *Ophthalmic Physiol Opt*. 2019;38:172–182.
49. Summers JA. The choroid as a sclera growth regulator. *Exp Eye Res*. 2013;114:120–127.
50. Zhang S, Zhang G, Zhou X, et al. Changes in choroidal thickness and choroidal blood perfusion in guinea pig myopia. *Invest Ophthalmol Vis Sci*. 2019;60:3074–3083.
51. Nickla DL, Wallman J. The multifunctional choroid. *Prog Retin Eye Res*. 2010;29:144–168.
52. Nickla DL, Zhu X, Wallman J. Effects of muscarinic agents on chick choroids in intact eyes and eyecups: evidence for a muscarinic mechanism in choroidal thinning. *Ophthalmic Physiol Opt*. 2013;33:245–256.
53. Delshad S, Collins MJ, Read SA, Vincent SJ. The time course of the onset and recovery of axial length changes in response to imposed defocus. *Sci Rep*. 2020;10(1):8322.

Investigative Ophthalmology & Visual Science

Downloaded from m.iovs.org on 05/02/2024